Dependence of CCN activity of less-volatile particles on the amount of coating observed in Tokyo

M. Kuwata*[1], Y. Kondo[1], M. Mochida[2†], N. Takegawa[1], and K.Kawamura[2]

1. Research Center for Advanced Science and Technology, the University of Tokyo, Tokyo, Japan
2. Institute of Low Temperature Science, Hokkaido University, Sapporo, Japan

† Now at Institute for Advanced Research, Nagoya University, Nagoya, Japan

Short title: CCN activity of less-volatile particles

* Corresponding author
e-mail: kuwata@atmos.rcast.u-tokyo.ac.jp

Last modified: January 5, 2007

submitted to JGR

Abstract

A novel observation system has been developed to measure cloud condensation nuclei (CCN) activity simultaneously with volatility of aerosol particles at 400°C. CCN/CN ratios were measured using a CCN counter and a condensation particle counter, and volatility was measured with a volatility tandem differential mobility analyzer (VTDMA). This system was connected to a hygroscopicity tandem differential mobility analyzer (HTDMA) in tandem to measure these properties of hygroscopicity-selected particles. These instruments were deployed in Tokyo in November 2004. In Tokyo, the dominant fraction of non-volatile cores at 400°C has been found to be black carbon (BC). Therefore, the number size distribution measured by VTDMA represents the mixing state of black carbon particles. The VTDMA measurement of hygroscopicity-selected particles revealed that most of the less-hygroscopic particles were less-volatile, while more-hygroscopic particles were more-volatile. CCN/CN ratios of less-volatile particles ($(CCN/CN)_{LV}$) are estimated from CCN activity and volatility measurements of less-hygroscopic particles. $(CCN/CN)_{LV}$ at SS $\geqq$ 0.5% are correlated with the decrease of peak diameter due to volatilization (Δd_m), and $(CCN/CN)_{LV}$ is nearly equal to unity at Δd_m = 10 nm. This result suggests that the CCN activity of BC particles significantly depends on the amount of coating.

1. Introduction

Black carbon (BC) is emitted to the atmosphere by incomplete combustion of fossil fuels and biomass. BC strongly absorbs solar radiation, leading to radiative heating of the atmosphere [*Haywood et al.*, 1997; *Myhre et al.*, 1998; *Jacobson*, 2001, 2002; *Ramaswamy et al.,* 2001]. It can also contribute to radiative forcing by changing snow and ice albedos [*Hansen and Nazarenko*, 2004]. Concentrations of BC are controlled by their transport and removal processes as well as emissions.

Removal of BC is dominated by wet deposition [e.g., *Jacobson*, 2004]. BC particles are hydrophobic and insoluble to water soon after emission because of their graphitic structure. However, it has been shown that BC becomes hydrophilic by surface oxidation [e.g., *Zuberi et al.,* 2005] and hygroscopic by condensation of secondary aerosol components [e.g., *Saathoff et al.,* 2003; *Sellegri et al.*, 2003]. Coated BC particles likely act as cloud condensation nuclei (CCN), although this point has not been clearly demonstrated by field measurements.

Global distributions of BC have been calculated by three-dimensional models, which incorporate emissions, transport, and removal of BC [*Cooke and Wilson,* 1996; *Chung and Seinfeld,* 2005; *Park et al.,* 2005]. One of the largest uncertainties in the model calculations is the estimate of the lifetime of BC. Almost all BC particles are assumed to be hydrophobic upon emission and become hydrophilic by the condensation of secondary aerosol compounds. The timescale of the evolution of BC properties is often given empirically in the form of an e-folding time, although the time scale can vary spatially and temporally [*Park et al.,* 2005]. For more accurate estimates of

the removal rate of BC, we need to improve our understanding of the coating process of BC and the dependence of its CCN activity on the state of coating.

It is advantageous to measure the aging of BC near its source regions considering the anticipated relatively short time-scales for the conversion of BC properties [*Saathoff et al.,* 2003;*Park et al.,* 2005]. In this study, relationships between CCN/CN ratio (CCN activity) and volatility at 400°C were investigated by deploying a CCN counter [*Roberts and Nenes*, 2005] and a volatility tandem differential mobility analyzer (VTDMA) [*Clarke et al.,* 2004; *Philippin et al.,* 2004] in Tokyo. *Kondo et al.* [2006] have shown that non-volatile particles at 400°C are nearly equivalent to BC in Tokyo. Therefore we can study the mixing states of BC particles using VTDMA. These measurements were performed for particles selected by a hygroscopicity tandem differential mobility analyzer (HTDMA) [*Mochida et al.*, 2006].

2. Critical supersaturation of particles containing insoluble cores

For the discussion of the CCN activity of BC, it is useful to calculate the CCN activity of a particle composed of an insoluble core and a single soluble component coating the core based on the Köhler theory. The equilibrium vapor saturation ratio of water (S) for particles with a dry diameter of d_{dry} and insoluble core diameter of d_{core} is expressed as a function of the diameter of the droplet (D_p), assuming the dry aerosol particle, insoluble core, and droplet are spherical in shape [*Seinfeld and Pandis,* 1998]

$$ln\ S = \frac{A}{D_p} - \frac{B(d_{dry}^3 - d_{core}^3)}{D_p^3 - d_{dry}^3} \quad \left(A \equiv \frac{4M_w\sigma}{RT\rho_w}\ B \equiv \nu\frac{M_w\rho_s}{\rho_w M_s}\right) \tag{1}$$

where σ is the surface tension, M_w and M_s are the molecular weight of water and solute, ρ_w and ρ_s are the density of water and solute, respectively, and ν is the van't Hoff factor.

The first term on the right-hand side of equation (1) represents the Kelvin effect. The Kelvin effect increases the equilibrium vapor pressure of water because of the surface tension of the droplet. The second term on the right-hand side shows Raoult's effect. Raoult's effect decreases the equilibrium vapor pressure due to the mixing of solute. When we consider a single particle, d_{dry} and d_{core} are constants. In this case, S depends strongly on D_p, because the variability of A, and B are relatively small. The calculated S as a function of D_p, the so-called Köhler curve, reaches a maximum value (S_{max}) at a certain D_p. The supersaturation (SS) corresponding to this value is called the critical supersaturation (critical SS = (S_{max} – 1)). The balance between the Kelvin and Raoult's effects determines the critical SS.

Figure 1 shows the critical SS of 100-nm particles as a function of d_{core}. The calculations were made for an insoluble core coated by ammonium sulfate and by glutaric acid. The volume fraction of the core (V_{core}/V_{total}) is also shown in Figure 1 as a function of d_{core}. If d_{core} < 80 nm, the volume fraction of the coating material is larger than V_{core}/V_{total}, and the critical SS does not strongly depend on d_{core}. In this region, the critical SS is mainly determined by the chemical composition of the coating material. If d_{core} > 80 nm, V_{core}/V_{total} exceeds the volume fraction of the coating material and

the critical SS increases with the increase of d_{core}. In this region, SS is sensitive to the amount of coating. Thus d_{core} = 80 nm is a good measure in separating the two regimes for the discussion of the CCN activity of internally mixed aerosol particles with d_{dry} = 100 nm. Table 1 shows the critical SSs of other compounds. Critical SSs are 2.1% at d_{core} = 100 nm for all compounds. In this case, the critical SSs depend only on the Kelvin effect.

3. Instruments

Figure 2a shows the experimental setup used in this study (HTDMA-CCNC/VTDMA system). In this system, size and mixing state (hygroscopicity) of aerosol particles were selected by HTDMA before the measurement of CCN activity and volatility. The HTDMA part of this system is described in detail by *Mochida et al.* [2006]. Therefore, only a brief description of HTDMA part is given here. Ambient particles were dried to a relative humidity (RH) < 4% by a diffusion-dryer. The poly-disperse dry particles in the sampled air were charged by a ^{241}Am bipolar charger, then their size was selected by a differential mobility analyzer (DMA1; TSI Model 3081). In this study, the sheath flow to sample flow ratio of all DMAs was set at 10:1. Observation results of 100-nm particles were analyzed in this study because the number concentration of CCN is highest at 90-140 nm during the observation period [*Mochida et al.*, 2006]. Classified particles were humidified to grow into larger particles depending on their hygroscopicity. The sheath flow of DMA2 was also humidified. The RH in the humidifier and DMA2 were set at 83% or 89% for the present study. The

precision of RH was 0.3%. The hygroscopic growth factor, denoted as g (RH), is defined as

$$g(\mathrm{RH}) = d_p(\mathrm{RH})/d_{dry} \qquad (2)$$

, where d_p(RH) is the particles diameter at a given RH.

The voltages applied to DMA2 were fixed to constant values to select particles with the corresponding g (RH) values. This voltage was scanned once per hour to measure the number distribution of g(RH). The humidified air was dried again by a Nafion dryer mounted downstream of DMA2. Then, classified dry particles were introduced to CPC1 (TSI model 3022A), a CCN counter (CCNC, Droplet Measurement Technologies) [*Roberts and Nenes, 2005*], and a heater. The total number concentration of the mono-disperse particle (condensation nuclei; CN) was measured by CPC1, and the CCN number concentrations were measured by the CCNC, respectively. The sample flow rate and the sheath flow rate of CCNC were set to 0.05 l/min and 0.45 l/min, respectively. The temperature gradient (ΔT) of the thermal gradient chamber in the CCNC was periodically cycled at four different values (3.6, 7.2, 10.8, and 16.2 K) for the measurements at different SS in the chamber. The SS corresponding to these ΔT values were calibrated by using dried ammonium sulfate ($(NH_4)_2SO_4$) particles. These particles were generated from an aqueous solution of ammonium sulfate by using an atomizer (TSI Model 3076). These particles were dried by a diffusion-dryer, and size selected by a DMA. Then, they were measured by a CPC and the CCNC to obtain the distributions of CCN/CN ratios. A sigmoid function

(equation (3)) was fitted to the experimental result,

$$\frac{CCN}{CN} = a + \frac{b}{1+exp(\frac{d_c - d_p}{c})} \quad (3)$$

where a, b, and c are constants obtained by fitting and d_c is the center diameter of the sigmoid function. d_c was assumed as the critical dry diameter of ammonium sulfate under the observation conditions. Note that the CCN/CN ratio is not necessarily 0.5 at d_c because of the existence of multiply charged particles and particle loss in the CCNC. In this study, CCN/CN ranged from 0.44 (ΔT = 16.2 K) to 0.55 (ΔT = 3.6 K) at d_c. The critical SS corresponding to the observed activation diameter was calculated by the Köhler theory at a temperature of 308 K. In this calculation, the osmotic coefficient of the aqueous solution was calculated by the Pitzer equation [*Pitzer and Mayorga*, 1973] as described by *Mochida et al*. [2006]. This SS was assumed to be equal to the SS in the CCNC. d_c and the SS corresponding to each ΔT are summarized in Table 2. The precisions of the CCN and CN number concentrations were estimated to be 2-10% and 1-4% from their temporal variation, respectively. Therefore, the precision of CCN/CN ratios was calculated to be 2-11%. The CCN/CN ratio for ammonium sulfate at 80 nm was 1.01. Therefore, the systematic error in the CCN/CN measurement at 100 nm was negligible.

The VTDMA consisted of a heater, two DMAs (TSI Model 3081), and a CPC (TSI Model 3022A). The VTDMA measures size distributions of non-volatile cores of the size-selected particles. The sample air was heated

to 400°C by a mantle heater wrapped around a stainless steel tube (3/8-inch outer diameter, 7-mm inner diameter, and 21 cm long). A thermocouple was attached to the outer wall at the center of the heated section. A proportional-integral-derivative (PID) controller (CAL3200, CAL controls) was used to maintain the temperature of the heater at 400±1°C. The average residence time of the sample air through the heated section was estimated to be 1.6 s at room temperature at the sample flow rate of 0.3 l/min. Particles with diameters prescribed by DMA1 lost their volatile components in the heated section. The size distributions of residual non-volatile cores were measured by the DMA3-CPC2 system.

The transport efficiency of particles through the heater is one of the important heater parameters. It was measured using sodium chloride (NaCl) particles because they do not evaporate at 400°C [*Brooks et al.,* 2002; *Philippin et al.,* 2004]. Poly-disperse NaCl particles were generated by an atomizer, dried by a diffusion-dryer, and size-selected by a DMA. The concentrations of the mono-disperse particles were measured by two CPCs operated in parallel. The same heater described above was mounted upstream of one of the CPCs. The transport efficiency of the heater, given as the particle concentration ratio measured by the two CPCs, was 0.98 for the range of particle diameters between 15 and 100 nm. The size dependence of transport efficiency was not detected in this size range.

Evaporation of volatile aerosol particles in the heating section was characterized by using $(NH_4)_2SO_4$ particles. Ammonium sulfate particles were generated and size-selected at 30, 50, 100, and 200 nm by the same method used for the calibration of the CCN counter. These particles were

introduced to the heater, and the size distributions downstream of the heater were measured by using a DMA and a CPC. Changes in the particle sizes at different temperatures were measured by this system. $(NH_4)_2SO_4$ particles began to evaporate at 175 °C irrespective to their initial diameters. Particles with diameters of 30 and 50 nm (100 and 200 nm) completely evaporated at 200°C (225°C). These volatilization temperatures are similar to those reported previously [*Brooks et al.,* 2002; *Paulsen et al.,* 2006]. This shows the consistency of our VTDMA measurements with the previous studies. The size dependence of the volatilization temperature may be due to the kinetics of volatilization. However, this effect was not so significant. *Kondo et al.* [2006] found that almost all inorganic and organic components measurable by an Aerodyne Aerosol Mass Spectrometer (AMS) evaporated by heating the sample tube at 400 °C. They have also observed that mass concentrations of the non-volatile particles of PM_1 have agreed quite well with those of elemental carbon simultaneously measured by a thermal-optical technique, indicating that BC was the main component of non-volatile cores.

There is a possibility that aerosol components evaporated in the heating section could re-condense in the cooling section [*Sakurai et al.,* 2003a; *Paulsen et al.,* 2006]. We have investigated this effect using the measurement system shown in Figure 2b. The heater, DMA, and CPC are the same used for the experiments described above. The thermodenuder (TSI Model 3065) is composed of a heating section and a gas adsorber downstream to remove volatilized compounds. Particles with a diameter of 100 nm were selected by DMA1. If the accumulation of volatilized

compounds onto non-volatile cores is significant, removal of the re-condensed compounds by the thermodenuder will decrease the diameter of the particles measured by the DMA2 and CPC. The temperatures of the thermodenuder were chosen to be room temperature (20°C) and 400°C to detect the possible effect of re-condensation onto non-volatile particles. The change of the mobility diameters caused by the heated thermodenuder was less than 1 nm. The particle concentration in the VTDMA heater (Figure 2a) was much lower (less than 50 particles/cm^3 for 100-nm particles) than those of ambient air (~10^4 particles/cc during the experiment) because of the charging efficiency of the charger and the classification by HTDMA. Therefore, re-condensation is negligible in this study.

The number size distributions of non-volatile cores at the inlet of DMA3 were derived from the data obtained by DMA3 and CPC2 (Figure 2a) using the STWOM inversion algorithm [*Markowski*, 1987]. The Stolzenburg-type DMA transfer function [*Stolzenburg*, 1988] and the counting efficiency of the CPC were taken into account for this calculation. The validity of the inversion procedure was estimated by TDMA measurement without the heater. The difference of number concentration between the inversion data (TDMA) and CPC1 data was less than 1% at all times. The random error of the peak diameter measured by DMA3-CPC2 system was less than 0.2 nm. The systematic difference in diameters was corrected when calculating the change of peak diameter caused by volatilization.

4. Field observations

The observation was made near the urban center of Tokyo during the period November 10-17, 2004. The sampling inlet was located approximately 20 m above ground level, and the instruments were located within a building at the Research Center for Advanced Science and Technology (RCAST) campus of the University of Tokyo (35.66°N, 139.66°E) in Japan. RCAST is located about 10 km west of the Tokyo Bay coastline and is near the southeastern edge of the Kanto Plain. The sampling location and general meteorological conditions are described in detail elsewhere [*Kondo et al.*, 2006]. More-detailed descriptions of the operational modes of HTDMA-CCNC/VTDMA system are given by *Mochida et al.* [2006].

5. Definitions of VTDMA parameters

In this section, some parameters used for the analysis of VTDMA data are defined. Figure 3 shows an example of the VTDMA data in Tokyo. This data was obtained prior to the observation by the HTDMA-CCNC/VTDMA system (See Appendix for more detailed information). The size distribution of the non-volatile core is bimodal. This bimodal size distribution has been observed at some urban sites, e.g., in Leipzig [*Philippin et al.,* 2004] and Aachen [*Wehner et al.*, 2004]. A fraction of 100-nm particles shows only a small (less than 20%) shift from their original dry diameter. These particles are mainly composed by non-volatile composition. This mode is defined as ‘less-volatile’ or ‘LV’. The particles containing relatively small non-volatile cores are called ’more-volatile’ or ‘MV’. These definitions have also been used in previous studies [*Sakurai et al.*, 2003a; *Wehner et al.*, 2004].

The number fraction of particles containing a non-volatile core (F_{NV}) was defined as the ratio of the number concentrations measured by VTDMA to those by CPC1. Some particles do not have the non-volatile cores measurable by the VTDMA (<15 nm). This fraction was defined as 'completely volatile' or 'CV.'

The normalized size distribution for the less-volatile mode is fitted by a Gauss function (f_{fit}; shaded area in Figure 3). The number fraction of more-volatile (MV) and completely volatile (CV) particles (F_{MV+CV}) is calculated from the number fraction of less-volatile particles (F_{LV}).

$$F_{MV+CV} = 1 - F_{LV} \quad (4a)$$

$$F_{LV} = \int f_{fit}\, d\, log d_p \quad (4b)$$

The peak diameter of the less-volatile mode shows slight changes from its original diameter by volatilization. This decrease in the peak diameter is defined as Δd_m. Terminology for VTDMA data used in this study is summarized in table 3.

6. CCN activity and volatility of hygroscopicity-selected particle

In this section, results obtained by the HTDMA-CCNC/VTDMA system are discussed. VTDMA and CCN data for hygroscopicity-selected particles are shown in section 6.1 and section 6.2, respectively. Section 6.3 shows the relationship between CCN activity and volatility of hygroscopicity-selected particles.

The hygroscopic growth of 100-nm particles for RH = 83% and 89% averaged over the observation period is plotted in Figure 4. The number size distributions of particles after humidification were bi-modal. One was a less-hygroscopic (LH) mode and the other was a more-hygroscopic (MH) mode. The volatility and CCN activity of hygroscopicity-selected particles were measured for g = 1.00, 1.11, 1.24, and 1.38 particles. For the present study, g = 1.00 and 1.11 are defined as less-hygroscopic, and g = 1.24 and 1.38 as more-hygroscopic.

6.1 Volatility of hygroscopicity-selected particles

Average number size distributions of non-volatile cores measured for different g (RH = 83% and 89%) are shown in Figure 5. The dominant part of the less-hygroscopic (g = 1.00) particles was in the LV mode. It should be noted that less-hygroscopic (g = 1.00) mode particles contain 10-17% completely volatile particles. Primary particles from lubricant oil emitted from motor vehicles may constitute some portion of these less-hygroscopic and completely volatile particles [*Sakurai et al.*, 2003b].

The fraction of MV particles increased with the increase in g (RH). For g (RH = 83% and 89%) = 1.11, both less-volatile and more-volatile particles were observed. In particular, for RH = 89%, a distinct peak of the LV mode was observed.

For g (RH = 83% and 89%) = 1.24 and 1.38, almost all non-volatile cores were in the MV mode. The size distributions of non-volatile cores for g = 1.24 and 1.38 particle are similar. Therefore it is likely that the

hygroscopicity of more-hygroscopic particles is mainly controlled by the chemical composition of the volatilized compounds [*Mochida et al.*, 2006]. *McMurry et al.* [1996] observed by electron microscope that less-hygroscopic particles were mainly composed of carbon and that their shapes were irregular, indicating that these particles were predominantly freshly emitted from diesel engines. They also showed that more-hygroscopic particles contained sulfur and oxygen. These results are qualitatively consistent with our analysis, which indicates that 1) less-hygroscopic particles were mainly composed of BC (LV particles), and 2) BC was not the main component of more-hygroscopic particles.

6.2 CCN/CN ratios of hygroscopicity-selected particles

The CCN/CN values measured as a function of *g* (RH) are shown in Figure 6. The CCN/CN values generally increased with *g* (RH). This is qualitatively consistent with the theoretical prediction [e.g., *Kreidenweis et al., 2005*; *Mochida et al.*, 2006]. For more-hygroscopic particles (*g* (RH = 83% and 89%) = 1.11-1.38), CCN/CN at SS = 0.5% was nearly equal to unity.

At SS = 0.2%, the CCN/CN ratios strongly depended on *g*. CCN/CN = 0.71 at *g* (RH =83%) = 1.24, but it was unity at *g* (RH =83%) = 1.38. As discussed in section 2, the critical SS for particle with $d_{\mathrm{core}} < 80$ nm (or MV mode) is expected to depend on the chemical composition of coating materials. Considering that *g* is a good indicator of chemical composition, and the similarity of size distributions of non-volatile cores (Figure 5), this result shows that CCN/CN (SS = 0.2%) for MV-mode particles is mainly

determined by the volatilized aerosol chemical composition. This point is discussed in detail by *Mochida et al.*(2006).

6.3 CCN activity of less-volatile particles

In this section, dependence of CCN activity of less-volatile particles on Δd_m is analyzed. This analysis was performed for g (RH = 83% and 89%) = 1.00 and g (RH = 89%) = 1.11 particles, because less-volatile peaks were clearly observed in these cases. The temporal variation of CCN/CN, F_{MV+CV}, and Δd_m of less-hygroscopic particles (g (RH = 83%) = 1.00) is shown in Figure 7. It can be seen that for Δd_m < 2-3nm, CCN/CN (SS = 0.5% and 0.8%) ratios are similar to F_{MV+CV}. This result suggests that the critical SSs of more- and completely volatile particles in the less-hygroscopic mode were lower than that of less-volatile particles. Δd_m increases during the daytime. When Δd_m > 3 nm, the CCN/CN ratios were often higher than F_{MV+CV}. This feature is more evident for SS = 0.8%. For more-quantitative analysis, the number fraction of CCN active particles of less-volatile particles for SS >0.5% was estimated by the following way. We assumed that all of more- and completely volatile particles have lower critical SSs than any less-volatile particles. Therefore, the number fraction of CCN active less-volatile particles in HTDMA selected particles (including MV and CV particles) is represented as (CCN/CN) - F_{MV+CV}. Then, the ratio of CCN active LV particles to all LV particles is calculated by dividing (CCN/CN) - F_{MV+CV} by F_{LV}

$$\left(\frac{CCN}{CN}\right)_{LV} = \frac{\left(\frac{CCN}{CN}\right) - F_{MV+CV}}{F_{LV}} \qquad (5).$$

$(CCN/CN)_{LV}$ is positive as long as CCN/CN is larger than F_{MV+CV}.

The $(CCN/CN)_{LV}$ ratios are compared with Δd_m in Figure 8. For SS = 0.5% and 0.8%, $(CCN/CN)_{LV}$ is nearly equal to zero for $\Delta d_m < 3$ nm. It begins to increase at Δd_m = 4-5 nm and approaches unity at about 10 nm. The increase of the $(CCN/CN)_{LV}$ is much sharper for SS = 0.8 % than for SS = 0.5%. For SS = 1.3%, $(CCN/CN)_{LV}$ was significantly higher than zero at Δd_m = 2 nm and exceeds 0.5 at Δd_m = 4 nm. The significance of this correlation is well above the precisions of the measurements of the CCN and VTDMA data described in section 3. The main component of non-volatile core is BC. Therefore, this result indicates that the CCN activity of BC particles for SS > 0.5% increases with the increase of the coating material. This result is qualitatively consistent with the theoretical prediction (section 2).

In general, BC particles are not spherical in shape [*e.g., Park et al., 2004*]. In addition, *McMurry et al.* [1996] showed that the shapes of less-hygroscopic particles are chain agglomerates or irregular. Therefore, dynamic shape factors before and after the volatilization are required to estimate the volume of volatilized materials. However, this kind of knowledge is not currently available. Because of this, it is difficult to interpret the changes of the CCN activity of less-volatile particles based on the Köhler theory.

Rogak et al. [1993] and *Park et al.* [2004] have found that the mobility

diameter of chain agglomerates is nearly equal to its projected area equivalent diameter observed by electron microscope. Therefore it may be possible to assume that 10 nm of Δd_m is nearly equal to 10 nm changes of the projected area equivalent diameter. If aerosol particles are spherical before and after volatilization and volatile components uniformly coated the non-volatile core, Δd_m = 10 nm corresponds to a coating thickness of 5 nm. Spherical particles have the shortest perimeter per unit of projected area among all kinds of shapes. Thus, the perimeter of non-spherical particles (e.g., chain agglomerates) per unit of projected area is longer than that of spherical particles. Therefore, the average coating thickness of non-spherical particles is expected to be thinner than that of spherical particles with the same projected area equivalent diameter. Thus, it is possible to conclude that a slight coating (< 5 nm) of volatile compounds on BC significantly increases its CCN activity.

7. Summary and conclusions

CCN activity and volatility of hygroscopicity-selected 100-nm particles were measured in Tokyo in November 2004 by combining a CCNC, VTDMA, and HTDMA. The number size distributions after humidification (RH = 83 and 89%) of these particles were bimodal: less-hygroscopic and more-hygroscopic modes. These hygroscopicity-selected particles were heated to 400°C to measure the size distributions of their non-volatile cores. The main component of non-volatile core at 400°C in Tokyo has been found to be BC. Less-hygroscopic mode particles were mostly less-volatile. On the other hand, more-hygroscopic particles were more- and completely-volatile.

The less-volatile particles in less-hygroscopic mode did not act as CCN at SS = 0.5, 0.8, and 1.3% when the change of peak diameter caused by volatilization (Δd_m) was smaller than ~3 nm. By contrast, the CCN/CN ratios of less volatile particles were significantly increased when Δd_m was larger than ~3 nm. This result suggests that the CCN activity of BC is highly sensitive to the amount of coating.

Acknowledgments. This work was supported by the Ministry of Education, Culture, Sports, Science, and Technology (MEXT), the Japanese Science and Technology Agency (JST), and the global environment research fund of the Japanese Ministry of the Environment. The measurements at RCAST in Tokyo were made as a part of Integrated Measurement Program for Aerosol and Oxidant Chemistry in Tokyo (IMPACT) campaigns. The IMPACT campaigns were conducted within the framework of the International Global Atmospheric Chemistry Project (IGAC), Mega-Cities: Asia. M. Kuwata thanks the Japan Society for the Promotion of Science (JSPS) for JSPS Research Fellowships for Young Scientists.

Author Addresses:

M. Kuwata, Y. Kondo, and N. Takegawa, Research Center for Advanced Science and Technology, University of Tokyo, 4-6-1 Komaba, Meguro-ku, Tokyo 153-8904, Japan. (kuwata@atmos.rcast.u-tokyo.ac.jp, kondo@atmos.rcast.u-tokyo.ac.jp, takegawa@atmos.rcast.u-tokyo.ac.jp)

M. Mochida, Institute for Advanced Research, Nagoya University, Furo-cho, Chikusa-ku, Nagoya 464-8601, Japan (e-mail: mochida@iar.nagoya-u.ac.jp)

K. Kawamura, Institute of Low Temperature Science, Hokkaido University, N19 W8, Kita-ku, Sapporo 060-0819, Japan (kawamura@pop.lowtem.hokudai.ac.jp)

References

Brooks, B. J., M. H. Smith, M. K. Hill, and C. D. O'Dowd (2002), Size-differentiated volatility analysis of internally mixed laboratory-generated aerosol, *J. Aerosol. Sci., 33,* 555-579.

Chung, S. H., and J. H. Seinfeld (2005), Climate response of direct radiative forcing of anthropogenic black carbon, *J. Geophys. Res., 110*, D11102, doi:10.1029/2004JD005441.

Clarke, A. D., Y. Shinozuka, V. N. Kapustin, S. Howell, B. Huebert, S. Doherty, T. Anderson, D. Covert, J. Anderson, X. Hua, K. G. Moore II, C. McNaughton, G. Carmichael, and R. Weber (2004), Size distributions and mixtures of dust and black carbon aerosol in Asian outflow: Physiochemistry and optical properties, *J. Geophys. Res., 109,* D15S09, doi:10.1029/2003JD004378.

Cooke, W. F., and J. J. N. Wilson (1996), A global black carbon aerosol model, *J. Geophys. Res., 101*(D14), 19,395-19,409.

Haywood, J. M., D. L. Roberts, A. Slingo, J. M. Edwards, and K P. Shine (1977), General circulation model calculations of the direct radiative forcing by anthropogenic sulfate and fossil-fuel soot aerosol, *J. Clim.*, *10*, 1562-1577.

Hansen, J., and L. Nazarenko (2004), Soot climate forcing via snow and ice albedos, *Proc. Natl. Acad. Sci., USA , 101*, 423-428.

Jacobson, M. Z. (2001), Strong radiative heating due to the mixing state of black carbon in atmospheric aerosols, *Nature*, *409*, 672-695.

Jacobson, M. Z. (2002), Control of fossil-fuel particulate black carbon and organic matter possibly the most effective method of slowing global

warming, *J. Geophys. Res.*, *107*(D19), 4410, doi:10.1029/2001JD001376.

Jacobson, M. Z. (2004), Climate response of fossil fuel and biofuel soot, accounting for soot's feedback to snow and sea ice albedo and emissivity, *J. Geophys. Res.*, 109, D21201, doi:10 1029/2004JD004945.

Kondo, Y., Y. Komazaki, Y. Miyazaki, N. Moteki, N. Takegawa, D. Kodama, S. Deguchi, M. Nogami, M. Fukuda, T. Miyakawa, Y. Morino, M. Koike, H. Sakurai, and K. Ehara (2006), Temporal variations of elemental carbon in Tokyo, *J. Geophys. Res.*, 111, D12205, doi:10.1029/2005JD006257.

Kreidenweis, S. M., K. Koehler, P. J. DeMott, A. J., Prenni, C. Carrico, and B. Ervens (2005), Water activity and activation diameters from hygroscopicity data – Part Ⅰ: Theory and application to inorganic salts, *Atmos. Chem. Phys.*, 5, 1357-1370

Markowski, G. R (1987), Improved Twomey's algorithm for inversion of aerosol measurement data, *Aerosol Sci. Technol., 7,* 127-141.

McMurry, P. H., M. Litchy, P. Huang, X. Cai, B. Turpin, W. D. Dick, and A. Hanson (1996), Elemental composition and morphology of individual particles separated by size and hygroscopicity with the TDMA, *Atmos. Environ, 30,* 101-108.

Mochida, M., M. Kuwata, T. Miyakawa, N. Takegawa, K. Kawamura, and Y. Kondo (2006), Relationship between hygroscopicity and cloud condensation nuclei activity for urban aerosols in Tokyo, *J. Geophys. Res.*, *111*, D23204, doi:10.1029/2005JD006980.

Myhre, G., F. Stordal, K. Restad, and I. S. Isaksen (1998), Estimation of the direct radiative forcing due to sulfate and soot aerosols, *Tellus*, *Ser. B*, *50*,

463-477.

Park, K., D. B. Kittelson, and P. H. McMurry (2004), Structural properties of diesel exhaust particles measured by transmission electron microscopy (TEM): Relationships to particle mass and mobility, *Aerosol Sci. Technol., 38,* 881-889.

Park, R. J., D. J. Jacob, P. I. Palmer, A. D. Clarke, R. J. Weber, M. A. Zondlo, F. L. Eisele, A. R. Bandy, D. C. Thornton, G. W. Sachse, T. C. Bond (2005), Export efficiency of black carbon aerosol in continental outflow: Global implications, *J. Geophys. Res., 110*, D11205, doi:10.1029/2004JD005432.

Paulsen, D., E. Weingartner, M. Rami Alfarra, and U. Baltensperger (2006), Volatility measurements of photochemically and nebulizer-generated organic aerosol particles, *J. Aerosol. Sci.,* 37, 1025-1051.

Philippin, S. A. Wiedensohler, and F. Stratmann (2004), Measurements of non-volatile fractions of pollution aerosols with an eight-tube volatility tandem differential mobility analyzer (VTDMA-8), *J. Aero. Sci., 35,* 185-203.

Pitzer, K.S., and G. Mayorga (1973), Thermodynamics of electrolytes. Ⅱ. Activity and osmotic coefficients for strong electrolytes with one or both ions univalent. *J. Phys. Chem.*, 77, 2300-2308.

Ramaswamy, V., O. Boucher, J. Haigh, D. Hauglustaine, J. Haywood, G. Myhre, T. Nakajima, G. Y. Shi, and S. Solomon (2001), Radiative forcing of climate change, in *Climate Change 2001: The Scientific Basis, Contribution of Working Group I to the Third Assessment Report of the Intergovernmental Panel on Climate Change*, edited by J. T. Houghton et

al., Cambridge Univ. Press, New York.

Roberts, G. C., and A. Nenes (2005), A continuous-flow streamwise thermal-gradient CCN chamber for atmospheric measurements, *Aerosol Sci. Technol., 39,* 206-221.

Rogak, S. N., R. C. Flagan, and H. V. Nguyen (1993), The mobility and structure of aerosol agglomerates, *Aerosol Sci. Technol., 18,* 25-47.

Saathoff, H., K. H. Naumann, M. Schnaiter, W. Schöck, O. Möhler, U. Schurath, E. Weingartner, M. Gysel, and U. Baltensperger (2003), Coating of soot and $(NH_4)_2SO_4$ particles by ozonolysis products of α-pinene, *J. Aerosol. Sci., 34,* 1297-1321.

Sakurai, H., K. Park, P. H. McMurry, D. D. Zarling, D. B. Kittelson, and P. J. Ziemann (2003a), Size dependent mixing characteristics of volatile and nonvolatile components in diesel exhaust aerosols, *Environ. Sci. Technol.*, 37, 5487-5495.

Sakurai, H., H. J. Tobias, K.H. Park, D. Zarling, K. S. Docherty, D. B. Kittelson, P. H. McMurry, and P. J. Ziemann (2003b), On-line measurements of diesel nanoparticle composition and volatility, *Atmos. Environ.*, 37, 1199-1210.

Sellegri, K., P. Laj, R. Dupuy, M. Legrand, S. Preunkert, and J.-P. Putaud (2003), Size-dependent scavenging efficiencies of multicomponent atmospheric aerosols in clouds, *J. Geophys. Res.*, *108*(D11), 4334, doi:10.1029/2002JD002749.

Seinfeld, J. H., and S. N. Pandis (1998), *Atmospheric Chemistry and Physics*, John Wiley & Sons, Inc, New York

Stolzenburg, M. R. (1988), An ultrafine aerosol size distribution measuring

system, Ph.D. Thesis, University of Minnesota, Minnesota

Wehner, B., S, Philippin , A. Wiedensohler, V. Scheer, R. Vogt (2004), Variability of non-volatile fraction of atmospheric aerosol particles with traffic influence, *Atmos. Environ.*, 38, 6081-6090.

Zuberi B., K. S. Johnson, G. K. Aleks, L. T. Molina, M. J. Molina, and A. Laskin (2005), Hydrophilic properties of aged soot, *Geophys. Res. Lett.,* 32, L01807, doi:10.1029/2004GL021496.

Appendix

VTDMA measurement shown in Figure 3

The experimental setup used to measure VTDMA data in Figure 3 is shown in Figure A1. This measurement was performed during November 8-9, 2004 at RCAST (Tokyo). Data was averaged over two days.

Figure Captions

Figure 1. Relationships between the size of insoluble cores and critical supersaturations (critical SSs). The calculation was performed for particles with a dry diameter of 100 nm. The solid line shows the critical SSs of particles composed of ammonium sulfate (coating material) and an insoluble core. The critical SSs of particles coated by glutaric acid are shown as the dashed line. The volume fraction of insoluble cores (V_{core}) is also shown in this figure. In the region where the core diameter is larger than 80nm, critical supersaturation strongly depends on core size. In the other region (core diameter < 80 nm) critical supersaturation is controlled by the solute composition.

Figure 2. a) HTDMA-CCNC/VTDMA system used in this study. b) The experimental setup used for the inspection of re-condensation of the heater.

Figure 3. An example of VTDMA data in Tokyo and the definitions of less-volatile and more-volatile particles

Figure 4. Average distribution of hygroscopic growth of 100-nm particles at RH = 83% (November 10-15, 2004) and at RH = 89% (November 17). The hygroscopic growth factor (*g*) is shown in upper part of the figure.

Figure 5. Size distribution of non-volatile cores included in hygroscopicity-selected 100-nm particles.

Figure 6. CCN/CN ratios of hygroscopicity-selected 100-nm particles. The upper and lower panels correspond to RH = 89% and RH = 83%, respectively.

Figure 7. Time series of CCN/CN ratios at SS = 0.5%, 0.8%, and F_{MV+CV} of 100-nm (g = 1.00 at RH = 83%) particles during November 10-12, 2004. The temporal variation of Δd_m of less-volatile particles is also shown in the figure.

Figure 8. Relationships between $(CCN/CN)_{LV}$ and Δd_m at SS = 0.5%, 0.8%, and 1.3%. Note that lines are guides to the eye.

Figure A1. The experimental setup used to measure the VTDMA data shown in Figure 3.

Table 1. Critical supersaturations (critical SSs) of 100-nm particles composed of an insoluble core and a single soluble coating compound. d_{core} is the diameter of the insoluble core. SS reported in %.

Compound	d_{core} = 0 nm	20 nm	40 nm	60 nm	80 nm	100 nm
Ammonium sulfate	0.14	0.14	0.14	0.15	0.19	2.1
Ammonium nitrate	0.13	0.13	0.14	0.15	0.19	2.1
Malonic acid	0.22	0.22	0.23	0.25	0.31	2.1
Glutaric acid	0.26	0.26	0.27	0.30	0.37	2.1
Levoglucosan	0.27	0.27	0.28	0.31	0.39	2.1

Table 2. Activation diameters of ammonium sulfate particles and corresponding SSs at each temperature gradient.

ΔT (K)	d_c (nm)	Critical SS (%)
3.6	74	0.2
7.2	41	0.5
10.8	31	0.8
16.2	23	1.3

Table 3: The definitions of parameters used for VTDMA data

Less-volatile (LV)	Particles that have a large (> 80 nm) non-volatile core
More-volatile (MV)	Particles that have a small (< 80 nm) non-volatile core
Non-volatile (NV)	Particles that have a non-volatile core (LV + MV)
Completely volatile (CV)	Particles that do not have a non-volatile core
F_{LV}	Number fraction of less-volatile particles
F_{MV+CV}	Number fraction of more- and completely volatile particles
F_{NV}	Number fraction of non-volatile particles
Δd_m	Change of peak diameter caused by volatilization (in this study, used only for LV)

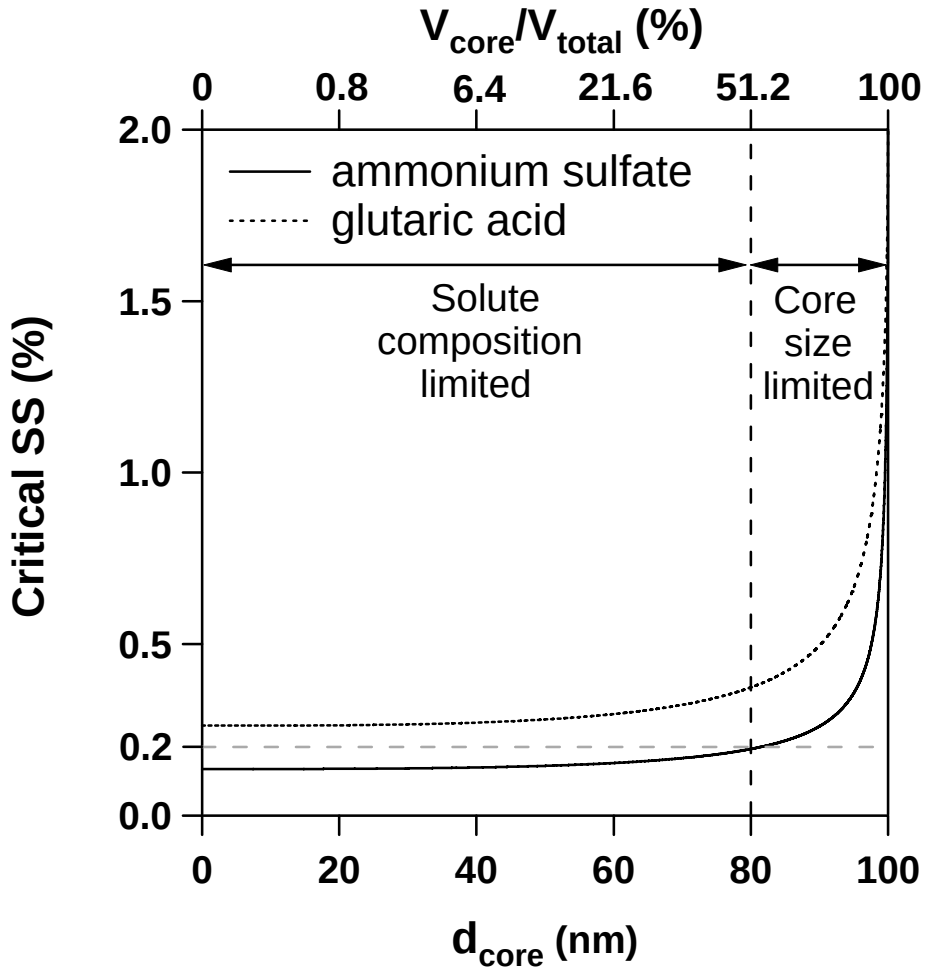
V_{core}/V_{total} (%)
0
0.8
6.4
21.6
51.2
100
2.0
1.5
1.0
0.5
0.2
0.0
ammonium sulfate
glutaric acid
Solute composition limited
Core size limited
Critical SS (%)
0
20
40
60
80
100
d_{core} (nm)

Figure 1

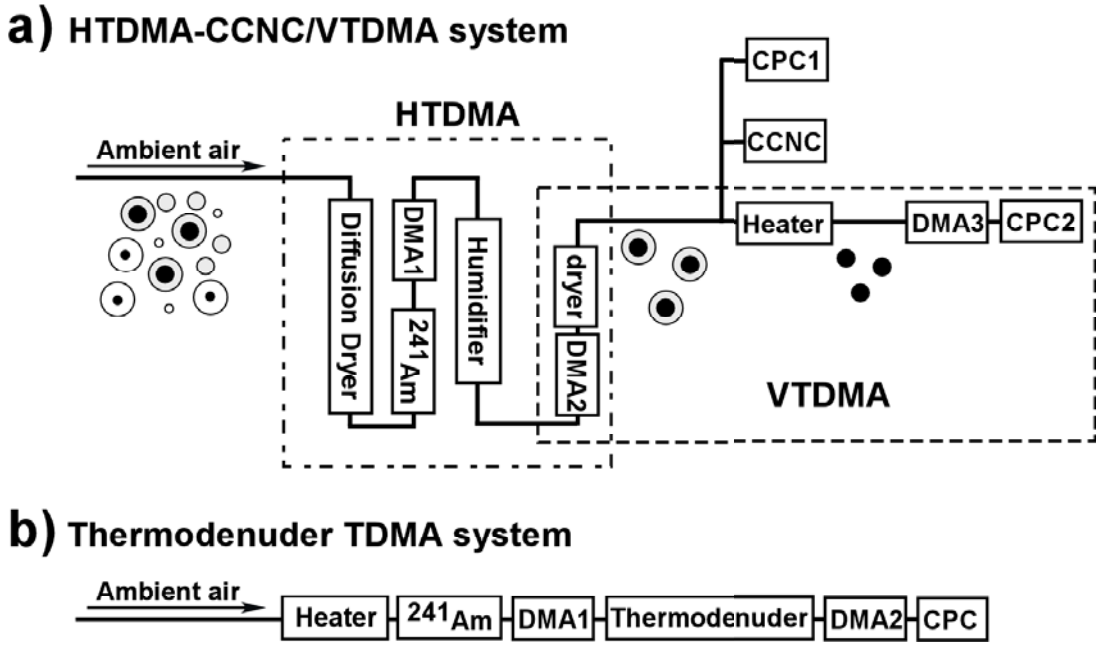
a) HTDMA-CCNC/VTDMA system
CPC1
HTDMA
CCNC
Ambient air
Heater
DMA3
CPC2
Diffusion Dryer
DMA1
Humidifier
dryer
241Am
DMA2
VTDMA
b) Thermodenuder TDMA system
Ambient air
Heater
241Am
DMA1
Thermodenuder
DMA2
CPC

Figure 2

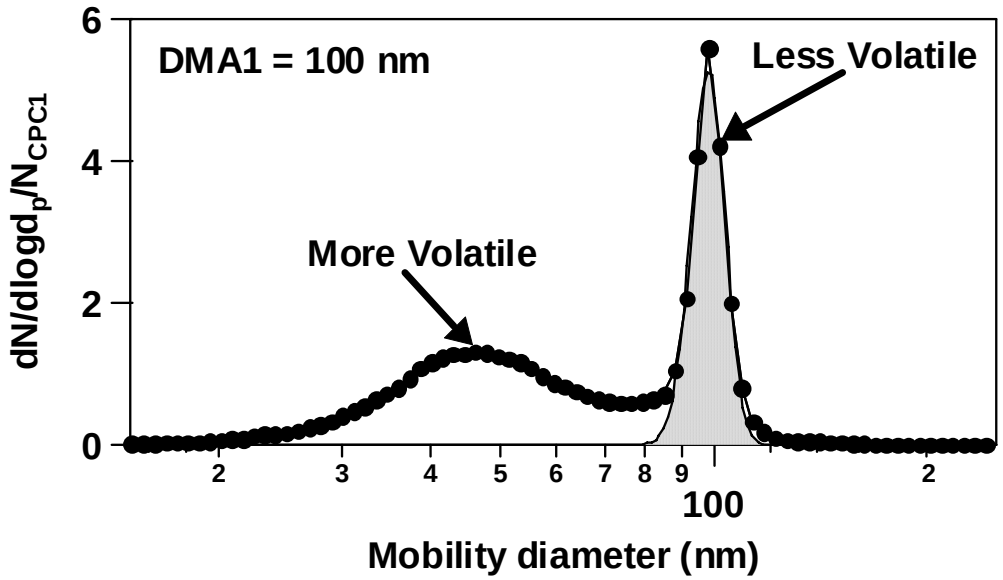
DMA1 = 100 nm
Less Volatile
More Volatile
dN/dlogd$_p$/N$_{CPC1}$
6
4
2
0
2
3
4
5
6
7
8
9
100
2
Mobility diameter (nm)

Figure 3

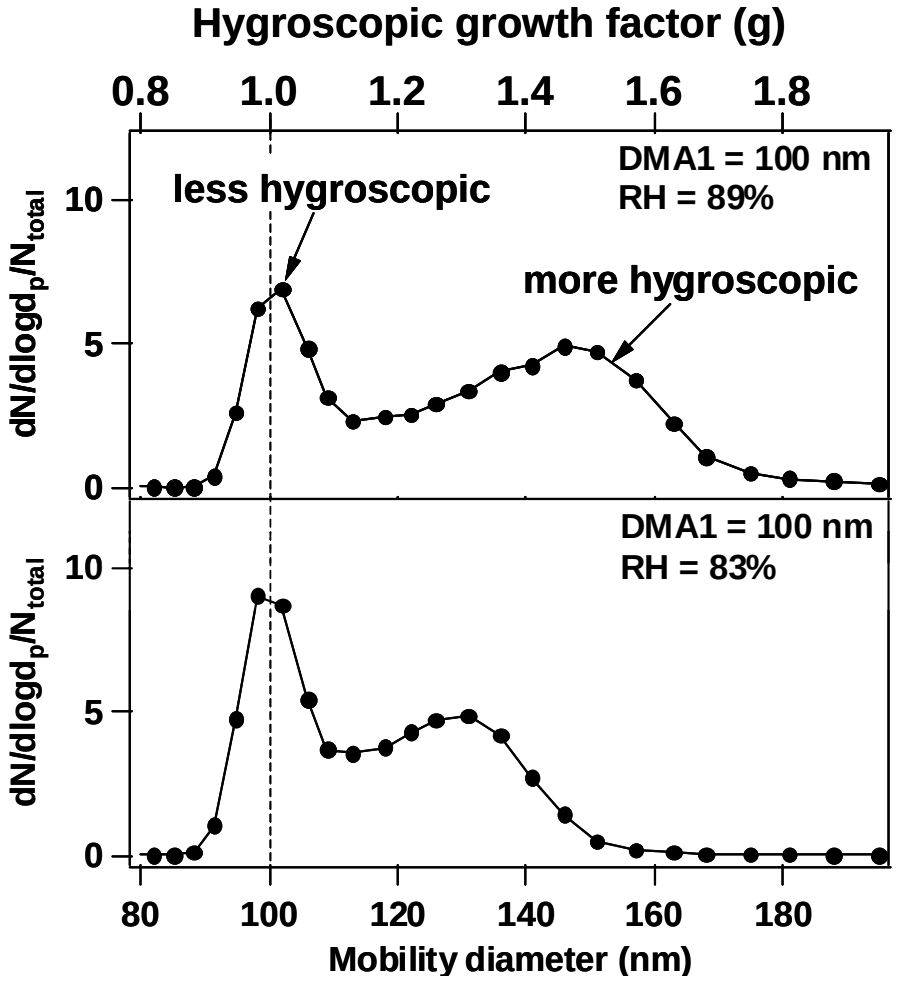
Hygroscopic growth factor (g)
0.8
1.0
1.2
1.4
1.6
1.8
DMA1 = 100 nm
RH = 89%
less hygroscopic
more hygroscopic
dN/dlogd$_p$/N$_{total}$
10
5
0
DMA1 = 100 nm
RH = 83%
dN/dlogd$_p$/N$_{total}$
10
5
0
80
100
120
140
160
180
Mobility diameter (nm)

Figure 4

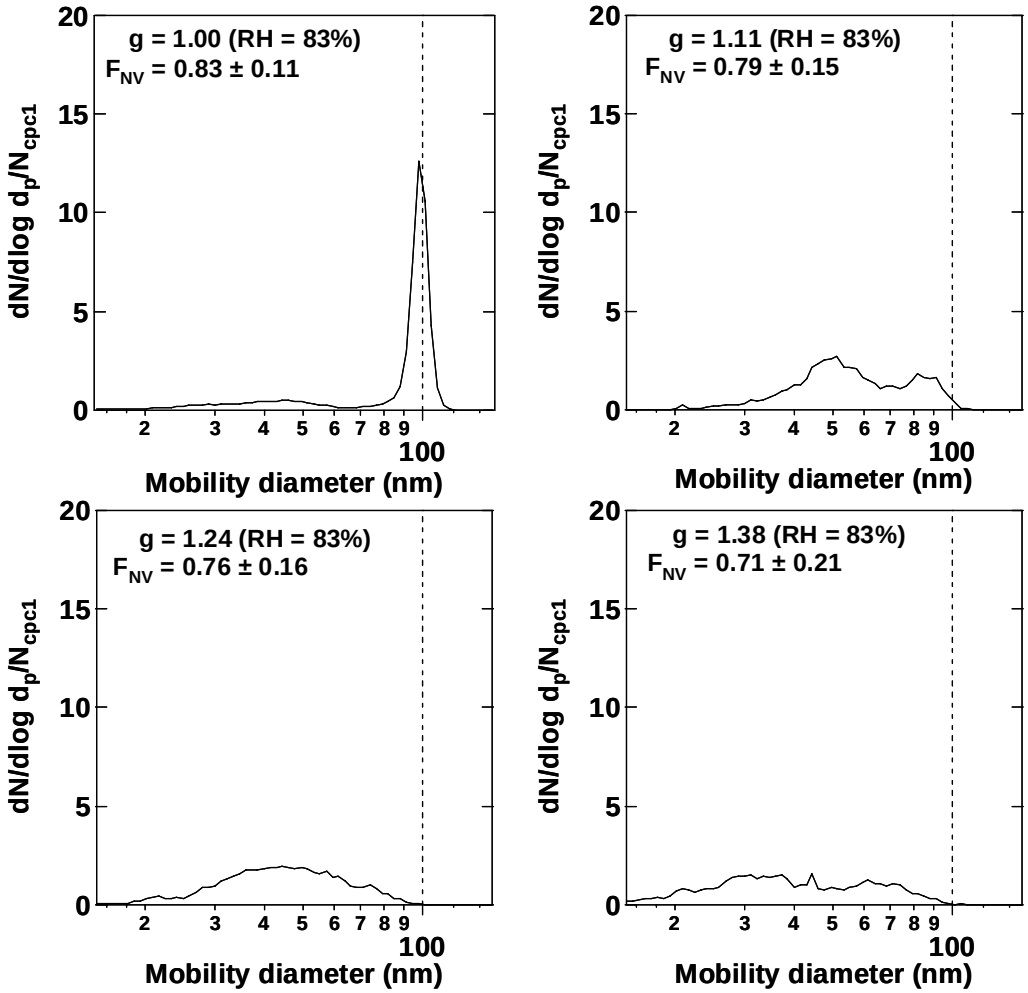
g = 1.00 (RH = 83%)
F_NV = 0.83 ± 0.11
g = 1.11 (RH = 83%)
F_NV = 0.79 ± 0.15
g = 1.24 (RH = 83%)
F_NV = 0.76 ± 0.16
g = 1.38 (RH = 83%)
F_NV = 0.71 ± 0.21
dN/dlog d_p/N_cpc1
Mobility diameter (nm)
0
5
10
15
20
2
3
4
5
6
7
8
9
100

Figure 5

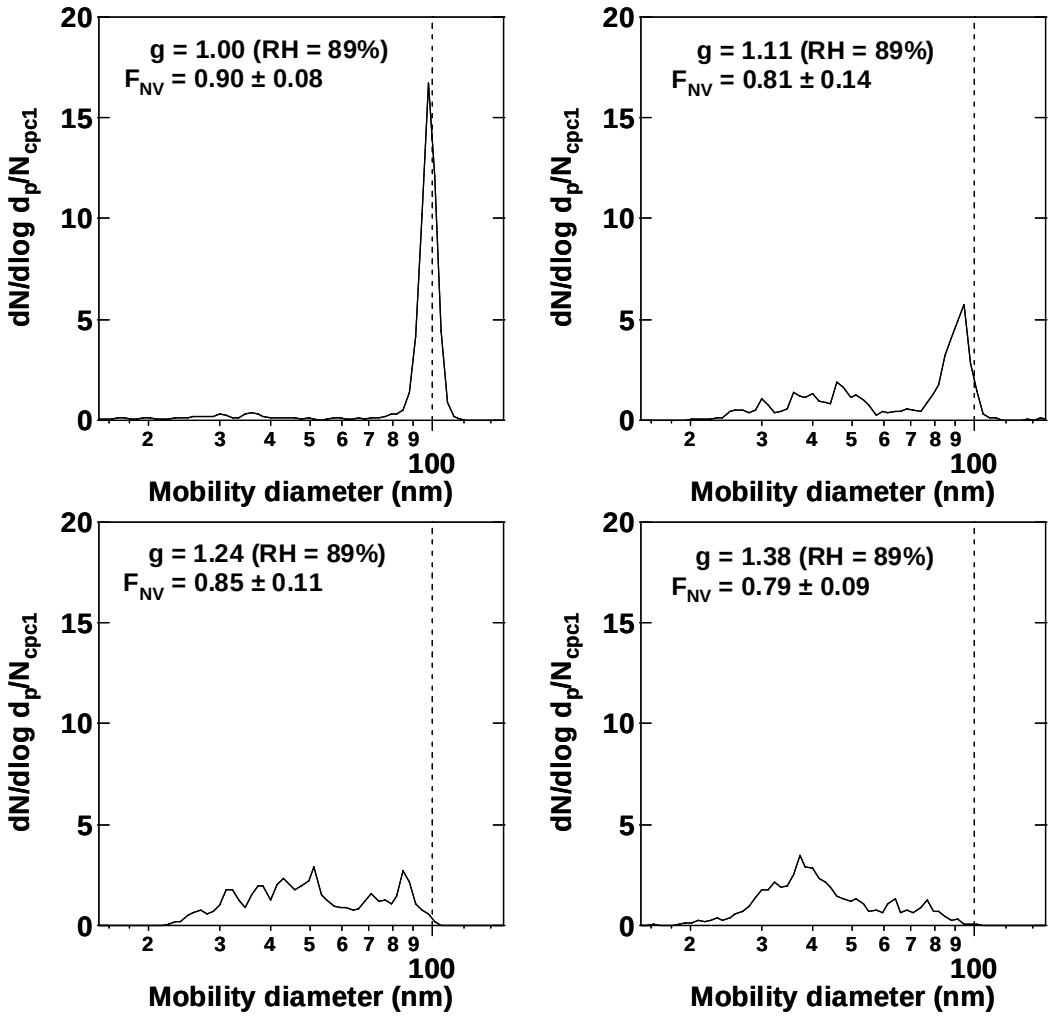

Figure 5 (continued)

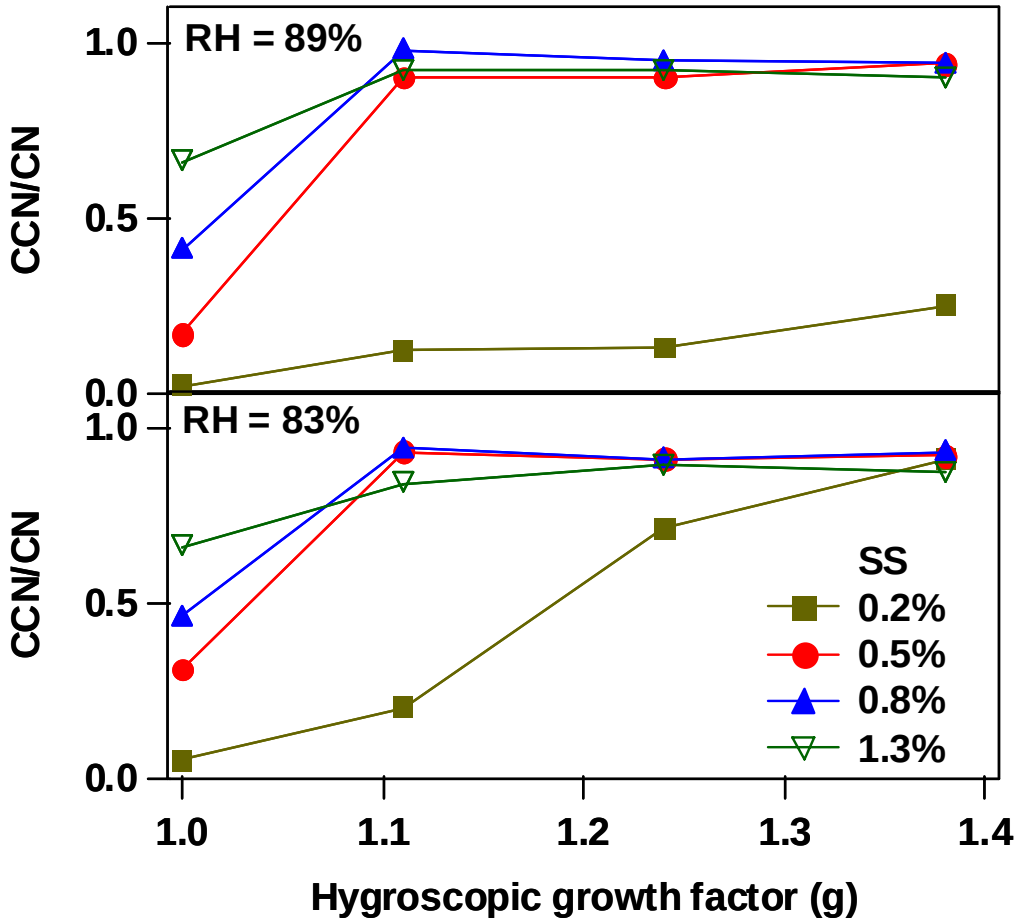
RH = 89%
RH = 83%
CCN/CN
CCN/CN
1.0
0.5
0.0
1.0
0.5
0.0
SS
0.2%
0.5%
0.8%
1.3%
1.0
1.1
1.2
1.3
1.4
Hygroscopic growth factor (g)

Figure 6

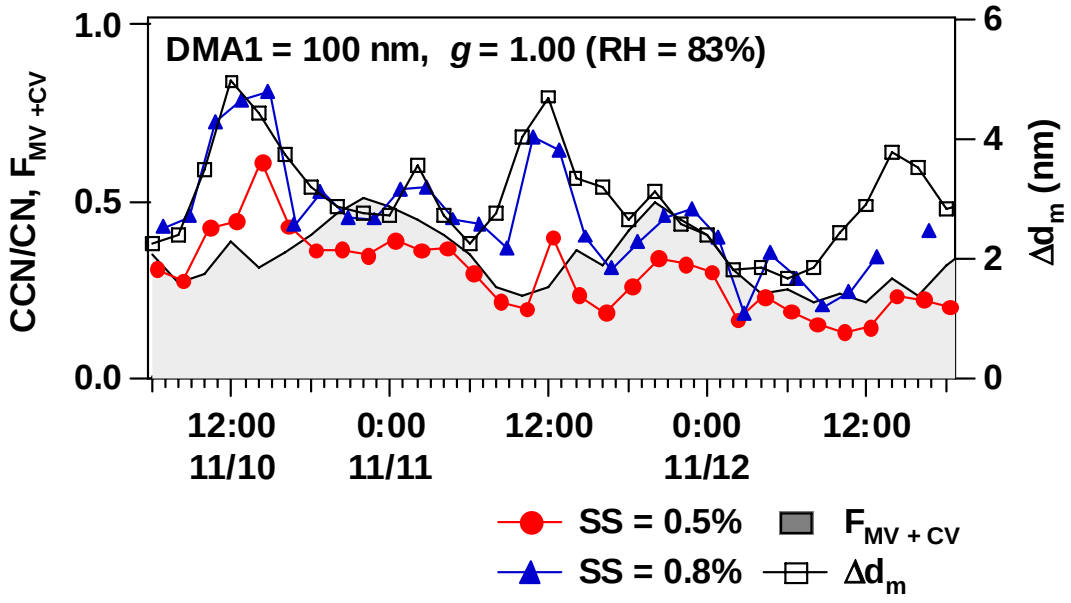
DMA1 = 100 nm, g = 1.00 (RH = 83%)
CCN/CN, F MV +CV
Δd m (nm)
1.0
0.5
0.0
6
4
2
0
12:00
11/10
0:00
11/11
12:00
0:00
11/12
12:00
SS = 0.5%
F MV + CV
SS = 0.8%
Δd m

Figure 7

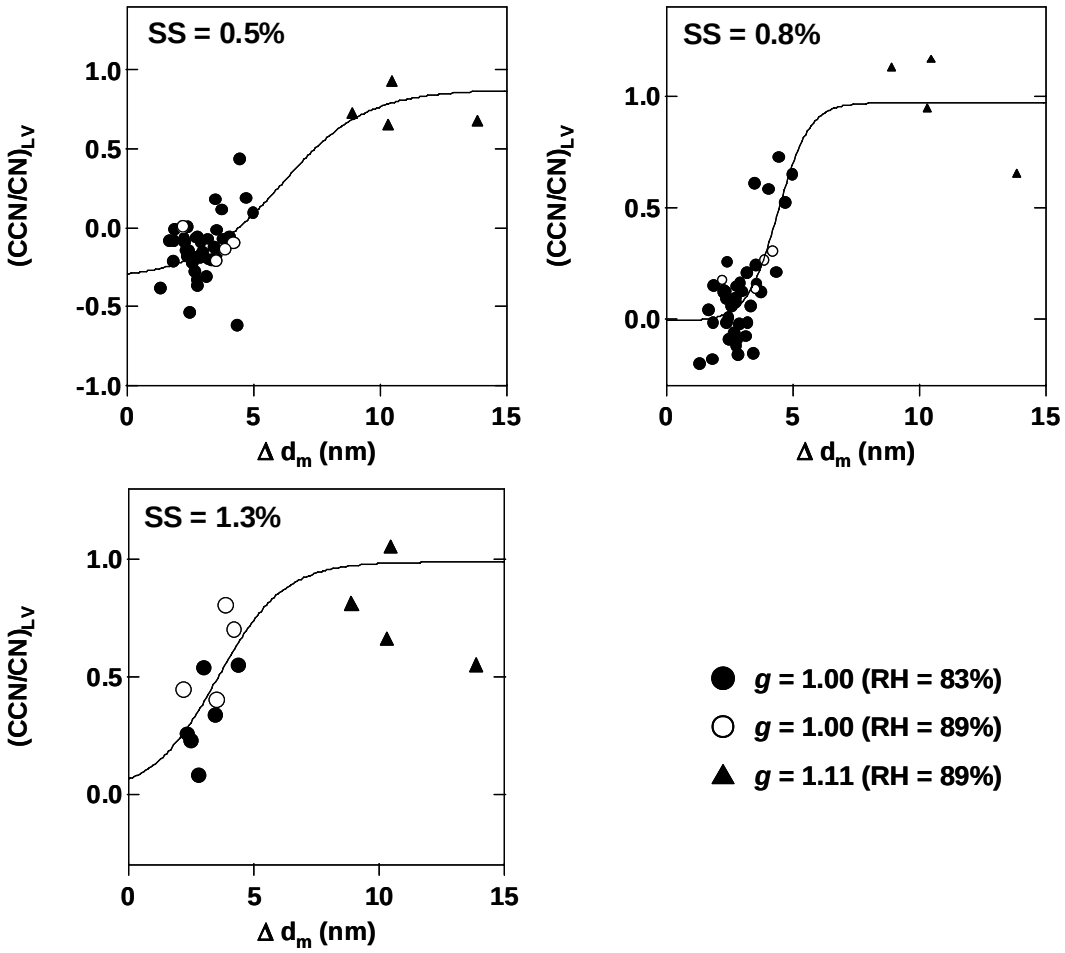

Figure 8

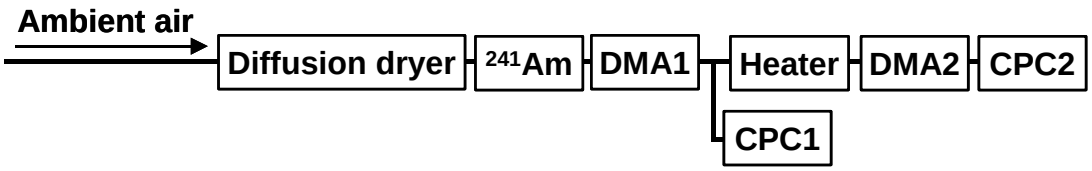
Ambient air
Diffusion dryer
241Am
DMA1
Heater
DMA2
CPC2
CPC1

Figure A1